Photoluminescence mechanism of Eu-doped molybdenum trioxide prepared by combustion synthesis

Y. ZHANG, M. RUAN, Q. ZHOU, X. MU, J. DU, E. XIE, Y. SHENG*, Z. ZHANG
School of Physical Science and Technology, Lanzhou University, Lanzhou 730000, PR China

Molybdenum trioxide (MoO_3) powders have been prepared with controllable Eu concentrations (1~7 at. %). The X-ray diffraction and Raman results show MoO_3 belongs to the orthorhombic phase. The intense sharp characteristic emission lines corresponding to Eu^{3+} intra-4*f* shell transitions of MoO_3 were observed in the photoluminescence emission spectra at room temperature and exhibited a maximum at the 3 at. % Eu sample. The optical bandgap of MoO_3 decreases from 3.26 to 3.14 eV as the Eu doping concentration increases from 1% to 7 at. %. Moreover, an energy transfer mechanism from MoO_3 host to Eu^{3+} ions is proposed.

(Received April 23, 2018; accepted November 29, 2018)

Keywords: Molybdenum trioxide, Optical materials and properties, Sintering, Energy transfer, Rare earths

1. Introduction

Rare earth-doped wide bandgap semiconductors have attracted much attention due to their sharp intra-4*f* optical transitions which extend from the infrared to the ultraviolet region and are much less sensitive to host and temperature as well as potential applications in biolables, optoelectronic devices, white light illumination, and solid state displays [1]. Among the various semiconductor hosts [2-6], molybdenum trioxide (MoO_3) is appealing because its direct wide bandgap allows large rare earth solid solubility and high luminescence efficiency while providing considerable chemical and physical stability [7, 8].

MoO_3 has a wide bandgap of 2.8-3.6 eV and three basic crystal structures (orthorhombic, monoclinic, hexagonal) [9]. The orthorhombic MoO_3 has anisotropic layered structure along the [010] direction and lacks inversion symmetry, rendering it as a suitable host. However, there are few studies on rare earth-doped MoO_3 [3, 7]. On the other hand, combustion is an economical and versatile method to prepare materials of high crystal quality. Herein, Eu-doped MoO_3 powders with controllable doping concentrations were prepared by combustion method. Intense red photoluminescence from Eu-doped MoO_3 powders were easily observable with the naked eye at room temperature. Moreover, the energy transfer mechanism between MoO_3 host and Eu^{3+} ions is discussed.

2. Experimental

Eu-doped MoO_3 powders were synthesized by the combustion method. The preparation process is briefly illustrated in Fig. 1(a). First, 0.5 g $MoCl_5$ (Aladdin, analytically pure) and different amounts (1, 3, 5, and 7 at. %) of Eu_2O_3 powder (Aladdin, analytically pure) were dissolved into 3 ml ethanol. Second, this mixture was magnetically stirred for several hours until dry and then put in a drying oven for another 30 h to obtain the precursor powder. Finally, Eu-doped MoO_3 were obtained by grinding and subsequent annealing the powders at 500°C for 2 h in air.

The obtained powders were examined by X-ray diffraction (XRD, Philips X'pert Pro, Cu Kα, 0.154056 nm) and energy dispersive X-ray spectroscopy (EDX) system (Hitachi S-4800). The Raman spectra were measured at room temperature by a micro-Raman spectroscopy (Jobin-Yvon HR 800) with a 325 nm He-Cd laser as the exciting source and a laser spot diameter of about 600 nm. Photoluminescence (PL) and Photoluminescence excitation (PLE) spectra were recorded through a fluorescent spectrophotometer (SHIMADZU RE-540PC).

3. Results and discussions

The surface morphologies of the pristine and Eu-doped MoO_3 powders are shown in Fig. 1(b-f). It can be seen that there are many layered bulks in micrometer size and few tiny particles in nanometer size. The larger Eu doping, the more particles are obtained. XRD patterns of the pristine and different Eu-doped MoO_3 powders are shown in Fig. 2(a). All the diffraction peaks can be well indexed to α-MoO_3 material (JCPDF: 05-0508) and no other phases are present. Compared to the pristine, the

diffraction peaks of the Eu-doped samples all shift slightly to the smaller angles, indicating the substitution of Mo ions (~0.73 Å) by large Eu ions (~1.09 Å). However, as the Eu doping concentration increases, the peaks shift to larger angles due to over Eu ions doping into the lattice space of MoO_3 (as shown in the inset of Fig. 2). Further, EDX results verify the controllable Eu doping of MoO_3 as listed in Table I, indicating the combustion method for doping is doable. The grain size of crystallites derived from the XRD peaks by the Scherrer formula are 36.2, 28.7, 33.1, 36.1, and 35.9 nm corresponding to the pristine, 1, 3, 5, and 7 at. % Eu-doped MoO_3 powders, respectively [10]. These results indicate that even high Eu doping does not change the crystal structure of MoO_3.

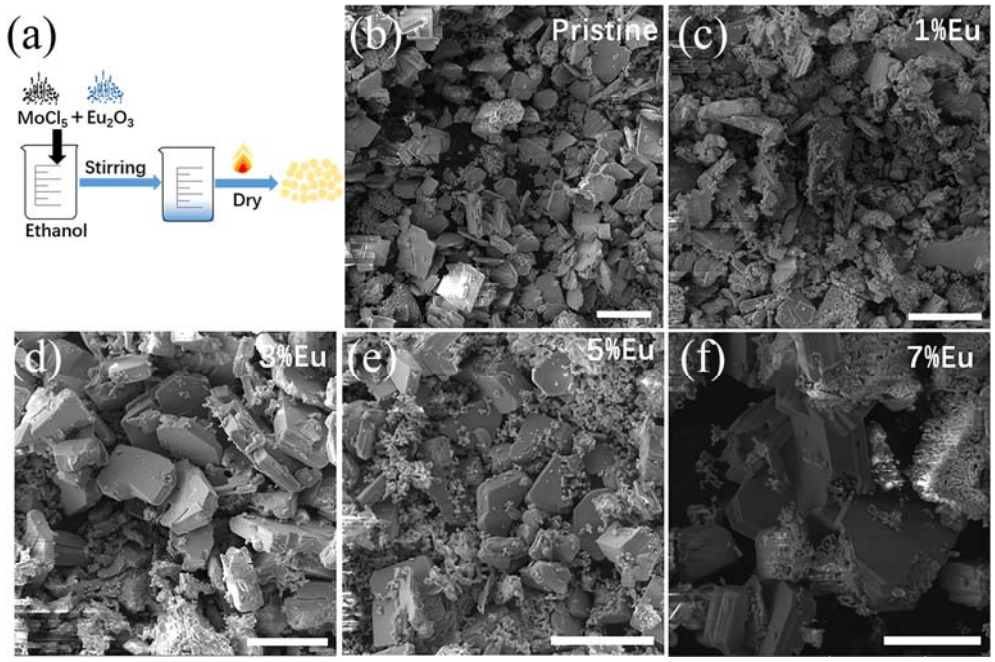

Fig. 1 (a) Schematic illustration of the preparation process. SEM images of the pristine (b), the 1% (c), 3% (d), 5% (e), and 7% (f) Eu-doped MoO_3 powders

The crystal structures of the MoO_3 samples were further eaxmined by Raman spectra as shown in Fig. 2 (b). The peak positions of all the samples are consistent with the previous literature data [11].

The peaks from 1000 to 600, from 400 to 200, and below 200 cm^{-1} can be attributed to the stretching, deformation, and lattice modes of α-MoO_3, respectively. It is worthy noting that the peaks don't change as the doping concentration increases, supporting the XRD results that the doping doesn't affect the crystal structure of α-MoO_3.

Table 1. The element ratio, grain size and optical bandgap of MoO_3

Sample	O-K at.%	Mo-L at.%	Eu-M at.%	O/Mo	Eu/Mo	Grain size (nm)	Optical bandgap (eV)
MoO_3	72.08	27.92	-	2.6	-	36.2	3.26
MoO_3: Eu 1%	76.02	23.70	0.28	3.2	1.2%	28.7	3.26
MoO_3: Eu 3%	73.28	25.75	0.97	2.8	3.8%	33.1	3.21
MoO_3: Eu 5%	67.79	30.57	1.64	2.2	5.4%	36.1	3.18
MoO_3: Eu 7%	79.43	19.30	1.27	4.1	6.6%	35.9	3.14

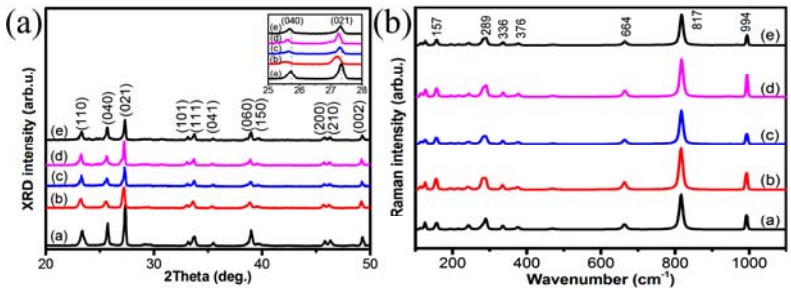

Fig. 2 (a) XRD patterns of the pristine (a), the 1% (b), 3% (c), 5% (d), and 7% (e) Eu-doped MoO_3 powders. (b) Raman spectra of the pristine (a), the 1% (b), 3% (c), 5% (d), and 7% (e) Eu-doped MoO_3 powders

Fig. 3 (a) (right) shows PL spectra of the pristine and the Eu-doped MoO_3 powders. All the doped samples show intense red emission under 340 nm excitation, being easily observable with the naked eye. The strongest emission peak at 619 nm corresponds to the $^5D_0 \rightarrow {}^7F_2$ transition of Eu^{3+} ions, which is a hypersensitive electric-dipole transition [5]. According to the parity selection rule, Eu^{3+} ions should occupy a site without inversion symmetry. The orthorhombic MoO_3 has P_{nma} symmetry. Therefore, there is a lack of inversion symmetry, thereby relaxing the parity selection rule and leading to the strongest emission at 619 nm of Eu^{3+} ions [12]. Other three weak PL peaks at 594, 655, and 703 nm are associated with the transitions from $^5D_0 \rightarrow {}^7F_1$, $^5D_0 \rightarrow {}^7F_3$, $^5D_0 \rightarrow {}^7F_4$, respectively. With the increase of doping concentration, the emission peaks of Eu^{3+} ions intensify up to 3%, and weaken for higher doping concentration, which is probably due to cross relaxation between Eu^{3+}-Eu^{3+} ions [13]. The full width at half-maximum of 619 nm peak of the 3% Eu-doped sample is about 11 nm, implying the red emission is sharp and well defined. In addition, the intensity ratio of the transition $^5D_0 \rightarrow {}^7F_2$ to the magnetic dipole allowed transition $^5D_0 \rightarrow {}^7F_1$ defines the red-to orange fluorescence factor (R/O factor) (or asymmetric ratio) and hence the strength of covalent/ionic bonding between Eu^{3+} ions and surrounding ligands. As can be seen from Fig. 3 (b) that the 3% Eu-doped sample has the maximum R/O factor of 3.60, which implies the 3% Eu-doped MoO_3 has the largest asymmetry and the highest covalency between Eu^{3+} ions and oxygen [14].

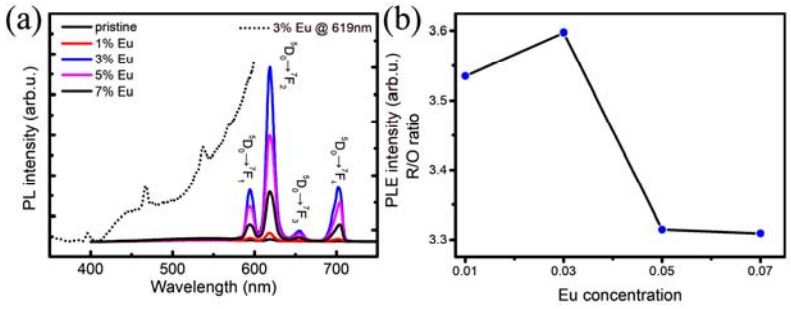

Fig. 3 (a) (right) PL spectra of the pristine and the Eu-doped MoO_3 powders under 340 nm excitation at room temperature. (left) PLE spectrum of the 3% Eu-doped MoO_3 powder monitored at 619 nm. (b) The R/O factor vs. the doping concentration.

In order to elucidate the energy transfer process between Eu^{3+} ions and MoO_3 host, the PLE spectrum and the optical bandgap of Eu-doped MoO_3 were explored. Fig. 3 (a) (left) shows the PLE spectrum of 3% Eu-doped MoO_3 powder for 619 nm emission, of which four distinct absorption peaks at 397, 467, 537, and 568 nm can be seen. In addition, the optical bandgap of MoO_3 can be deduced from the absorbance spectra of the pristine and the Eu-doped MoO_3 powders (Fig. 4 (a)). By plotting the absorption coefficient ($(\alpha h\nu)^2$) as a function of photon energy ($h\nu$) and extrapolating the linear portion to $\alpha h\nu = 0$ (the inset of Fig. 4 (a) [2], the optical bandgaps are 3.26, 3.26, 3.21, 3.18, and 3.14 eV, corresponding to the pristine, the 1, 3, 5, and 7 at. % Eu-doped MoO_3 powders as listed in Table I, respectively. Therefore, the 397 nm peak of the PLE spectrum can be ascribed to the bandgap absorption of MoO_3 host matrix and the other three peaks of PLE are corresponding to the 4*f*-4*f* transitions of Eu^{3+} ions. A simple energy diagram is depicted in Fig. 4 (b) to illustrate the possible mechanism of emission and energy transfer process. Upon above-gap excitation, most of the excited electrons in MoO_3 will relax to Eu^{3+} ions and the Eu^{3+} ions will also absorb photon energy through $^7F_0 \rightarrow {}^5D_2$, $^7F_0 \rightarrow {}^5D_1$, and $^7F_0 \rightarrow {}^5D_0$ transitions, after nonradiative energy transfer process like multiphonon relaxation, finally the 594, 619, 655, 703 nm emissions are obtained.

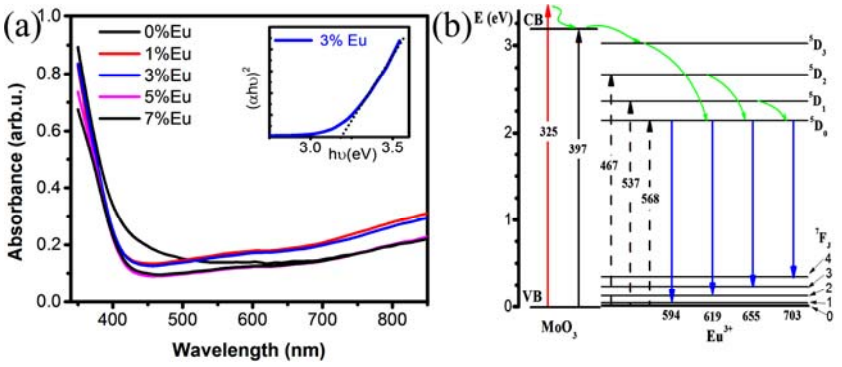

Fig. 4 (a) Absorbance spectra of the pristine and the Eu-doped MoO3 powders. The inset shows the absorption coefficients as a function of photon energy of 3% Eu-doped MoO_3 powder to deduce the optical bandgap. (b) Schematic diagram of the energy transfer process between MoO3 host and 4f shell of Eu^{3+} ions. The lines with arrows denote possible transitions: vertical lines – absorption or emission, curved lines - nonradiative energy transfer process

4. Conclusions

In summary, the controllable Eu-doped orthorhombic MoO_3 materials have been prepared by a facile combustion method. The grain sizes of crystallites are 36.2, 28.7, 33.1, 36.1, and 35.9 nm corresponding to the pristine, 1, 3, 5, and 7 at. % Eu-doped MoO_3, respectively. Raman spectra further demonstrate the the Eu doping doesn't affect the crystal structure of α-MoO_3. The intense red photoluminescence ascribed to Eu^{3+} intra-4*f* shell transitions were observed at room temperature. An energy transfer mechanism from MoO_3 host to Eu^{3+} ions is proposed. These results suggest that MoO_3 can be a suitable host material for rare-earth-based optoelectronic devices.

Acknowledgments

This work was supported by the National Natural Science Foundation of China (No. 51302122), the Fundamental Research Funds for the Central Universities (Nos: lzujbky-2016-133, lzujbky-2017-k21), the National Fund for Talent Training in Basic Science of the National Natural Science Foundation of China.

References

[1] A. J. Steckl, J. H. Park, J. M. Zavada, Materials Today **10**(7-8), 20-27 (2007).
[2] Z. X. Zhang, X. J. Pan, L. X. Liu, Z. W. Ma, H. T. Zhao, L. Jia, E. Q. Xie, J. Appl. Phys. **105**(1), 016101 (2009).
[3] Bin Dong, Zi An Li, Baosheng Cao, Naisen Yu, Mengtao Sun, Opt. Commun. **284**(10–11), 2528 (2011).
[4] Boxu Xu, Pei Wang, Xiaoqi Meng, Kaishun Zou, J. Lumin. **175**, 78 (2016).
[5] Meiqi Chang, Yanhua Song, Ye Sheng, Jie Chen, Haifeng Zou, Phys. Chem. Chem. Phys. **19**(26), 17063 (2017).
[6] Jinyuan Zhou, Dengfei Song, Hao Zhao, Xiaojun Pan, Zhenxing Zhang, Yanzhe Mao, Yujun Fu, Tao Wang, Erqing Xie, J. Lumin. **157**, 119 (2015).
[7] Pingyuan Ren, Xiaozhi Liu, Ke Zhang, Peng Zhang, Feng Teng, Zhenxing Zhang, Erqing Xie, Pengxun Yan, Mater. Lett. **122**, 320 (2014).
[8] O. Kamoun, A. Boukhachem, M. Amlouk, S. Ammar, J. Alloys. Compd. **687**, 595 (2016).
[9] Liqiang Mai, Fan Yang, Yunlong Zhao, Xu Xu, Lin Xu, Bin Hu, Yanzhu Luo, Hangyu Liu, Materials Today **14**(7–8), 346 (2011).
[10] Paul F. Fewster, X-ray scattering from semiconductors, 2nd edition, World Scientific Publishing, 2003.
[11] Hathai Sinaim, Dong Jin Ham, Jae Sung Lee, Anukorn Phuruangrat, Somchai Thongtem, Titipun Thongtem, J. Alloys. Compd. **516**(0), 172 (2012).
[12] Melis Gökçe, Ufuk Şentürk, Deniz K. Uslu, Gözde Burgaz, Yüksel Şahin, Aytaç Gürhan Gökçe, J. Lumin., **192**, 263 (2017).
[13] Huaqiang Wu, Carl B. Poitras, Michal Lipson, Michael G. Spencer, Janet Hunting, Francis J. DiSalvo, Appl. Phys. Lett. **88**(1), 011921 (2006).
[14] Jianguo Zhao, Huigao Duan, Ziwei Ma, Tao Wang, Changcheng Chen, Erqing Xie, J. Appl. Phys. **104**(5), 053515 (2008).

*Corresponding author. shengyzh@lzu.edu.cn